Finite Element Modeling of Shunt Reactors Used in High Voltage Power Systems

Tu P. Minh
School of Electrical Engineering
Hanoi University of Science and Technology
Hanoi, Vietnam

Hung B. Duc
School of Electrical Engineering
Hanoi University of Science and Technology
Hanoi, Vietnam

Nam P. Hoai
School of Electrical Engineering
Hanoi University of Science and Technology
Hanoi, Vietnam

Trinh Tr. Cong
School of Electrical Engineering
Hanoi University of Science and Technology
Hanoi, Vietnam

Minh B. Cong
School of Electrical Engineering
Hanoi University of Science and Technology
Hanoi, Vietnam

Bao D. Thanh
University of Quy Nhon
Qui Nhon, Binh Dinh,Vietnam

Vuong D. Quoc
School of Electrical Engineering
Hanoi University of Science and Technology
Hanoi, Vietnam

Abstract—Shunt reactors are important components for high-voltage and extra high voltage transmission systems with large line lengths. They are used to absorb excess reactive power generated by capacitive power on the lines when no-load or under-load occurs. In addition, they play an important role in balancing the reactive power on the system, avoiding overvoltage at the end of the lines, and maintaining voltage stability at the specified level. In this paper, an analytical method based on the theory of magnetic circuit model is used to compute the electromagnetic fields of shunt reactors and then a finite element method is applied to simulate magnetic field distributions, joule power losses, and copper losses in the magnetic circuit. In order to reduce magnetic flux and avoid magnetic circuit saturation, it is necessary to increase the reluctance of the magnetic circuit by adding air gaps in the iron core. The air gaps are arranged along the iron core to decrease the influence of flux fringing around the air gap on shunt reactors' total loss. Non-magnetic materials are often used at the air gaps to separate the iron cores. The ANSYS Electronics Desktop V19.R1 is used as a computation and simulation tool in this paper.

Keywords-shunt reactors; air gaps; inductance; Joule power losses; copper losses; finite element method

I. INTRODUCTION

The shunt reactor is a widely used component that improves the stability and efficiency in power transmission systems. High-voltage and extra-high-voltage power transmission systems usually have relatively large line lengths. Under no or small load, parasitic capacitance will appear in the line, its value is quite large especially in long lines, which will increase the voltage along the line, causing overvoltage at the end of the line. This phenomenon is known as the Ferranti effect [1-3]. In order to maintain voltage stability at the specified level, it is necessary to use shunt reactors to absorb the excess reactive power generated by the line capacitance, balancing the reactive power in electrical systems [3-5].

The construction of shunt reactors is correlated with power transformers such as windings, magnetic circuits, insulation structures, or shields. The shunt reactor can be considered as a transformer working with no load. However, the main difference in the shunt reactor, is that each phase is a winding. In order to reduce the magnetic flux and avoid the saturation of the magnetic circuit, the reluctance is increased by creating horizontal gaps. This leads to increased energy stored in the gap areas. The volume of gaps depends on the reactive power and the selected magnetic inductance. However, the gaps are also reasons to flux fringing along the gaps [6-8] which increases the power losses in the shunt reactor. The gap needs to be divided into several smaller gaps to reduce the effect of the flux fringing, thereby reducing power losses in the shunt reactor.

Shunt reactors have been extensively used, e.g. for the compensation reactive power in a power system [3, 4], the interaction between shunt reactors and the power system in different transient conditions [8, 9], and the vibration analysis [9, 10]. In this research, an analytical method based on the theory of magnetic circuit model and finite element method (FEM) were used to compute and simulate the electromagnetic parameters of shunt reactors.

II. ANALYTIC METHOD

A. Shunt Reactor Modeling

The model of the shunt reactor is presented in Figure 1. Thanks to this model, when ignoring the leakage flux, it is possible to divide the magnetic circuit into different parts and is given in the equivalent magnetic circuit in Figure 2.

Corresponding author: Vuong D. Quoc (vuong.dangquoc@hust.edu.vn)

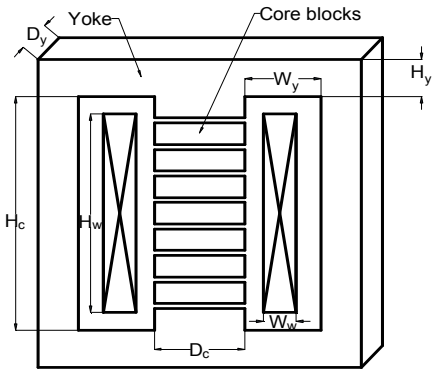

Fig. 1. Modeling of the shunt reactor.

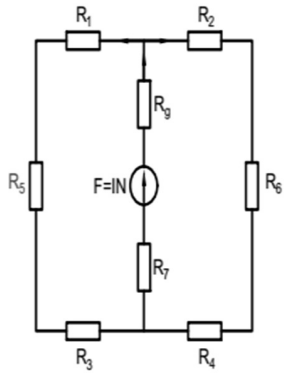

Fig. 2. Equivalent magnetic circuit.

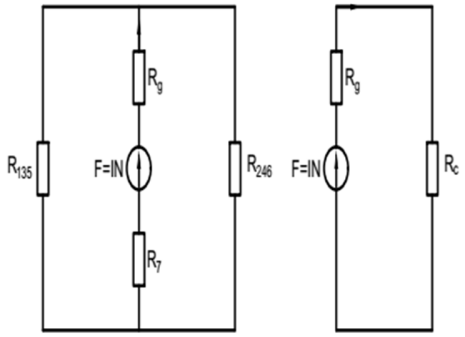

Fig. 3. Reduced equivalent magnetic circuits.

The electromotive force (EMF) generated by the current I in the N turns of windings is denoted by $F = I.N$ (A.turn). Due to the symmetry of the magnetic circuit, the reluctances of the upper and lower yokes are determined by (1):

$$R_1 = R_2 = R_3 = R_4 = \frac{1}{\mu}\frac{2W_y+D_c+H_y}{2.H_y.D_y} \quad (1)$$

The reluctances of two sides and of the middle core can be defined by (2) and (3):

$$R_5 = R_6 = \frac{1}{\mu}\frac{H_c+H_y}{H_y.D_y} \quad (2)$$

$$R_7 = \frac{1}{\mu}\frac{4.(H_c+H_y-l_g)}{\pi D_c^2} \quad (3)$$

where μ is the permeability of the ferromagnetic material and l_g is the total gap length in the core. W_y, D_c, H_y, and D_y are the parameters given in Figure 1.

The diagram in Figure 2, it can be transformed into Figure 3. The equivalent reluctance of the reduced equivalent magnetic circuits is defined as:

$$R_c = R_7 + \frac{R_2+R_4+R_6}{2} = \frac{4.(H_c+H_y-l_g)}{\mu.\pi.D_c^2} + \frac{2W_y+D_c+2H_y+H_c}{2\mu.H_y.D_y} \quad (4)$$

The reluctance of the gap in the iron core is calculated as:

$$R_g = \frac{1}{\mu_0}\frac{4.l_g}{\pi.D_c^2} \quad (5)$$

The reluctance R_c in (4) is very small in comparison with the reluctance of the air gaps. Thus, the R_c can be neglected in the equivalent magnetic circuit.

B. Parameter Computations

In this part, the single phase shunt reactor of 30.33MVar ($500/\sqrt{3}$ and 50Hz) is considered in Figure 1. The idea of this step is to increase the reluctance by adding air gaps in the iron core. The volume of the air gaps is defined via equations based on the magnetic circuit model. It should be noted that the volume of the air gaps depends on the main parameters of the shunt reactor, i.e. reactive power, magnetic flux density, winding inductance, frequency, and energy storage in the winding space air gaps. The reactive power is expressed by the electric current and the voltage, i.e.:

$$Q = U.I \quad (6)$$

The winding resistance is normally very small in comparison with the inductance, thus it can be neglected when defining parameters of the magnetic circuits. The electromagnetic force and the electric current are defined as:

$$E = \left(\frac{2\pi}{\sqrt{2}}\right).f.N.\phi_m = \left(\frac{2\pi}{\sqrt{2}}\right).f.N.B_m.A_g \quad (7)$$

$$I = \frac{.R_g}{N} = \left(\frac{1}{\sqrt{2}}\right)\frac{B_m.l_g}{\mu_0.N} \quad (8)$$

where $\phi_m, B_m, A_g, l_g, R_g$ and μ_0 are respectively the maximum magnetic flux, maximum flux density, area of the air gap, length of the air gap, air gap reluctance, and air permeability.

Based on (7) and (8), the volume V_g is determined by the air gap length l_g:

$$V_g = A_g.l_g = \frac{Q}{\frac{\pi}{\mu_0}.f.B_m^2} \quad (9)$$

where the reactive power, magnetic flux, and frequence are considered as constants and so the volume of the air gaps is also a constant. Hence, the A_g and l_g will be defined based on this air gap, because they are two important parameters that can be affected directly to total power losses and the size of shunt reactors.

If the air gap area is equal to the core area, the dimension of core is written as:

$$D_c = \sqrt{\frac{4.A_g}{\pi}} \quad (10)$$

From (10), the yoke area can be defined as:

$$D_y = D_c,\ H_y = \frac{A_g}{2.D_y} \quad (11\text{ a-b})$$

and the winding inductance is computed by the reactive power and voltage as:

$$L = \frac{U^2}{\omega.Q} \quad (12)$$

or

$$L = N^2.\mu_0.\left(\frac{A_g}{l_g}\right) = N^2.P_g \quad (13)$$

From (13), the turns of the winding and the magnetic window are calculated as:

$$N = \sqrt{\frac{L}{\mu_0.(\frac{A_g}{l_g})}},\qquad A_w = W_w.H_w = \frac{N.I}{k_u.J} \quad (14\text{ a-b})$$

where k_u is the filled factor of the windings in the magnetic window and J is the electric current density.

In addition, it is seen that in a region around the air gap appears flux fringing as presented in Figure 4.

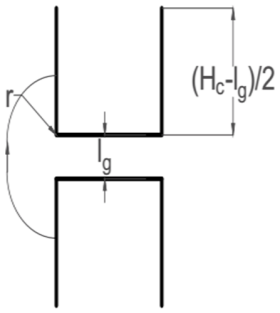

Fig. 4. Modeling of fringing flux around the air gap.

Thus, the flux fringing is defined as [7]:

$$\phi_f = \int B.dA = \int_0^{\frac{H_c-l_g}{2}} \frac{\mu_0.F}{l_g+\pi.r}.\pi.D_c\,dr \quad (15)$$

The magnetic conducting can be defined via the MMF and fringing flux as:

$$P_f = \mu_0.D_c.\ln\left(1+\frac{\pi(H_c-l_g)}{2.l_g}\right) \quad (16)$$

The magnetic conducting taking the flux fringing into account is expressed as:

$$P_{gf} = P_g + P_f \quad (17)$$

The turn number is finally written as:

$$N = \sqrt{\frac{L}{P_c+P_{gf}}} \quad (18)$$

The copper and core losses are defined as:

$$P_{Cu} = I^2.k_f.R_{dc} \quad (19)$$

for

$$R_{dc} = \rho.\frac{l_{tb}}{A_{Cu}} = \rho.\frac{\pi.N.(D_c+W_w+2.b_{cw})}{A_{Cu}}$$

$$P_{Fe} = k_p.\left(p_t.G_t + p_g.G_g\right) \quad (20)$$

where k_p is the auxiliary loss factor, p_t and p_g are the losses in the core and yoke, and G_t and G_g are the weights of the core and yoke. The calculated results of the shunt reactor are given in Table I.

TABLE I. OBTAINED RESULTS OF THE SHUNT REACTOR BY THE ANALYTIC METHOD

Parameters	Notation	Results
Reactive power	Q (MVAr)	30.33
Rated voltage	U (kV)	$500/\sqrt{3}$
Rated current	I (A)	105
Total inductance	L (H)	8.7457
Core dimension	D_c (mm)	673
Core height	H_c (mm)	1758
Total air gap	l_g (mm)	363
Turn number	N (vòng)	2166
Winding width	W_w (mm)	248
Winding height	H_w (mm)	1488
Copper loss	P_{Cu} (kW)	51.9038
Iron loss	P_{Fe} (kW)	20.4260

III. FINITE ELEMENT METHOD

A. Canonical Magnetodynamic Problem

In this problem, the characteristic size of the studied domain Ω with boundary $\partial\Omega = \Gamma = \Gamma_h \cup \Gamma_e$, is considered much less than the wave-length $\lambda = c/f$ in each medium. Hence, the displacement current density is negligible. The problem is described by Maxwell's equations [11-16]:

$$\text{curl}\,\boldsymbol{e} = -\partial_t \boldsymbol{b},\ \text{curl}\,\boldsymbol{h} = \boldsymbol{j}_s,\ \text{div}\boldsymbol{b} = 0 \quad (21\text{a-b-c})$$

and the behavioral relations of materials:

$$\boldsymbol{b} = \mu\boldsymbol{h},\ \boldsymbol{j} = \sigma\boldsymbol{e} \quad (22\text{a-b})$$

where $\boldsymbol{b}$ is the magnetic flux density, $\boldsymbol{h}$ is the magnetic field, $\boldsymbol{e}$ is the electric field, μ is the magnetic permeability, σ is the electric conductivity, $\boldsymbol{j}$ is the eddy current density belonged to the conducting part Ω_c ($\Omega_c \subset \Omega$), and $\boldsymbol{j}_s$ is the imposed electric current density defined in the non-conducting Ω_c^C, with $\Omega_c = \Omega_c \cup \Omega_c^C$.

Equations (21a) and (21b) are to be solved with the Boundary Conditions (BCs) that the tangential component of the magnetic field on BC is $\boldsymbol{n}\times\boldsymbol{h}|_{\Gamma_e}$, for $\boldsymbol{n}$ being the unit normal exterior to Ω.

B. Magnetic Vector Potential Formulations

Based on the Maxell's equations along with the constitutive relations in (22), the weak form of Ampere' law (22b) is written [5, 11, 13] as:

$$\int_\Omega \boldsymbol{h}\cdot\text{curl}\,\boldsymbol{a}'\,d\Omega + \int_{\Gamma_h}\boldsymbol{n}\times\boldsymbol{h}\cdot\boldsymbol{a}'\,d\Gamma_h = \int_{\Omega_s}\boldsymbol{j}_s\cdot\boldsymbol{a}'\,d\Omega_s, \forall\,\boldsymbol{a}' \in \boldsymbol{H}_e^0(\text{curl};\Omega) \quad (23)$$

In order to satisfy strongly the lower part of the Tonti's diagram [14], the constitutive laws (23 a-b) have to be introduced in (12), i.e.:

$$\frac{1}{\mu}\int_{\Omega} \boldsymbol{b}\cdot \operatorname{curl}\boldsymbol{a}'\, d\Omega - \sigma\int_{\Omega} \boldsymbol{e}\cdot\boldsymbol{a}'\, d\Omega_c + \int_{\Gamma_h} \boldsymbol{n}\times\boldsymbol{h}\cdot \boldsymbol{a}'\, d\Gamma_h = \int_{\Omega_s} \boldsymbol{j_s}\cdot\boldsymbol{a}'\, d\Omega_s, \forall\, \boldsymbol{a}' \in \boldsymbol{H}_e^0(\operatorname{curl};\Omega) \quad (24)$$

By substituting $\boldsymbol{b} = \operatorname{curl}\boldsymbol{a}$ and $\boldsymbol{e} = -(\partial_t \boldsymbol{a} + \operatorname{grad} v)$ into (24), we get:

$$\frac{1}{\mu}\int_{\Omega} \operatorname{curl}\boldsymbol{a}\cdot\operatorname{curl}\boldsymbol{a}'\, d\Omega - \sigma\int_{\Omega_c}\partial_t\boldsymbol{a}\cdot\boldsymbol{a}'\, d\Omega_c + \sigma\int_{\Omega_c}\operatorname{grad} v\cdot\boldsymbol{a}'\, d\Omega_c + \int_{\Gamma_h}\boldsymbol{n}\times\boldsymbol{h}\cdot\boldsymbol{a}'\, d\Gamma_h = \int_{\Omega_s}\boldsymbol{j_s}\cdot\boldsymbol{a}'\, d\Omega_s$$
$$\forall\, \boldsymbol{a}' \in \boldsymbol{H}_e^0(\operatorname{curl};\Omega) \quad (25)$$

where $\boldsymbol{H}_e^0(\operatorname{curl};\Omega)$ is a curl-conform function space defined on Ω containing the basis functions for $\boldsymbol{a}$ as well as for the test function $\boldsymbol{a}'$(at the discrete level, this space is defined by edge finite elements). The electric scalar potential v is only defined in Ω_c.

The energy and inductance are now defined via the magnetic flux density and magnetic intensity. This can be done in post-processing, i.e.:

$$W_m = \frac{1}{2}\int_{\Omega} \boldsymbol{b}\cdot\boldsymbol{h}\, d\Omega,\ L = \frac{2.W_m}{I^2} \quad (26)$$

IV. NUMERICAL TEST

The calculated parameters of the shunt reactor given in Table I were checked with the FEM developed in Section III, with the help of the Ansys Maxwell 3D. Ansys Maxwell is a part of the Ansys Electronics software package created by Ansys Inc. A 3D model of the single phase shunt reactor with 8 air gaps is depicted in Figure 5. The distribution of the current density in the windings is pointed out in Figure 6.

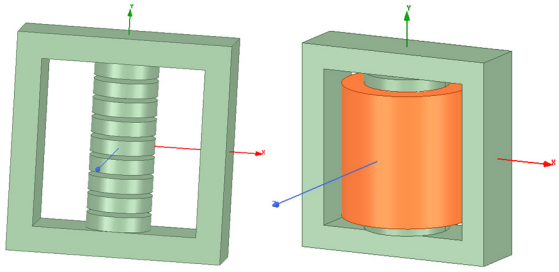

Fig. 5. 3D model of the single phase shunt reactor.

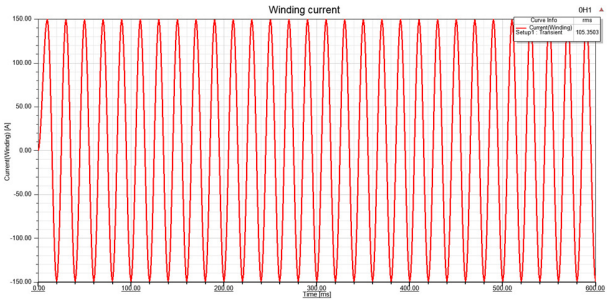

Fig. 6. Distribution of the current in the winding.

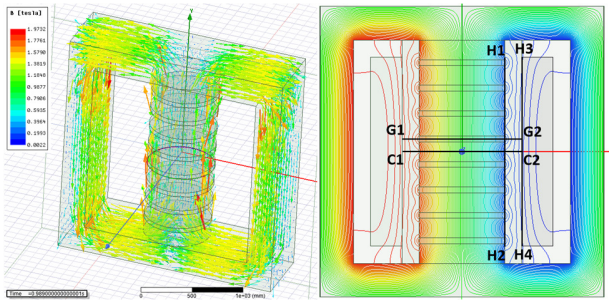

Fig. 7. Magnetic flux density and magnetic flux line distribution.

The magnetic flux density and flux line distribution in the magnetic core are presented in Figure 7. In Figure 7, C1-C2 is the line at the middle of core blocks, G1-G2 is the line at the middle of air gap, H1-H2 is the line along the core height and H3-H4 is the line along the height of windings. The flux density variation along C1-C2 and H1-H2 are depicted in Figure 8 and 9 respectively. The flux density obtains maximum values near the edges and the corners of the air gaps (Figure 8) and it is distributed equally along the H3-H4 as shown in Figure 10.

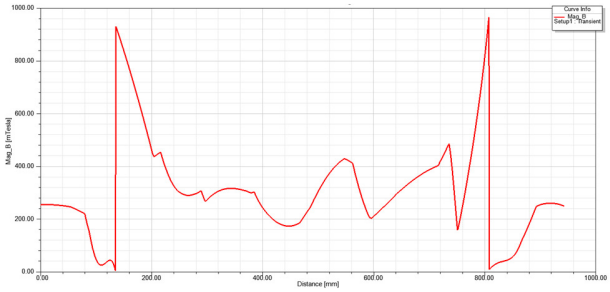

Fig. 8. Flux density variation along the line at the middle of core blocks.

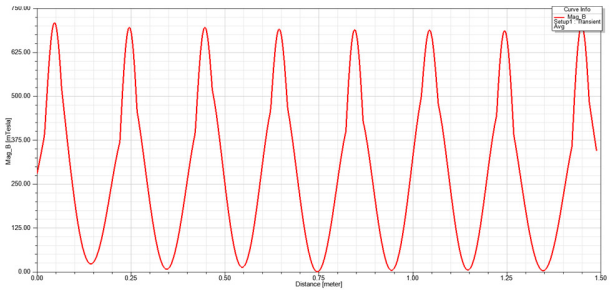

Fig. 9. Flux density variation along the height of the core.

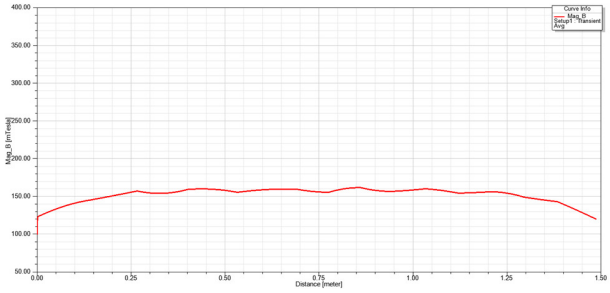

Fig. 10. Flux density variation along the height of the windings.

Copper and core losses are shown in Figures 11 and 12 respectively. The copper losses in the windings determined by the FEM are 52.2859kW whereas the analytical result in Table I is 51.9038kW, with the error being lower than 1%. It is seen that in order to avoid the increase of losses due to the fringing flux acting on the windings near to the gap area, it is necessary to divide a bigger gap into several smaller gaps. This reduces the fringing flux around the air gaps.

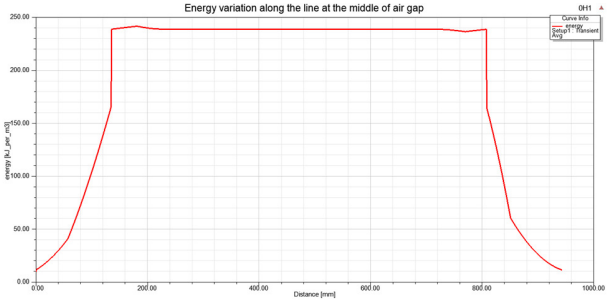

Fig. 11. Energy variation along the line G1-G2 at the middle of the air gap.

Fig. 12. Copper losses in the windings.

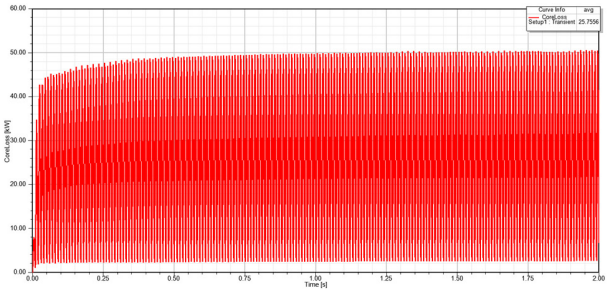

Fig. 13. Core losses of the shunt reactor.

TABLE II. INDUCTANCE VALUES COMPARISON BETWEEN FEM AND THE ANALYTIC METHOD

Parameters	FEM	Analytic method	Error (%)
Total inductance L (H)	8.6619	8.7457	0.96%
Gap inductance L_g (H)	5.6953	5.7819	1.50%
Fringing inductance L_f (H)	2.0017	1.2212	63.91%
Leakage inductane L_L (H)	0.9578	0.8746	9.51%

Similarly, the core losses obtained by FEM are 25.7556kW while the analytical result is 20.4260kW, with an error equal to 26%. It can be seen that the analytical method cannot determine exactly the distribution of the magnetic flux density in the core and yoke, because the magnetic flux density at different positions leads to different losses. In addition, the fringing flux component at the gap areas towards the steel foil in accordance with the direction of magnetization at different angles causes eddy currents that increase the losses in the cores. Table II presents the result comparison between the FEM and the analytic method. The error on the gap inductance between the two methods is 1.5% and lower than 1% for total inductance. However, the inaccuracy on the fringing flux is very big (63.91%), because the fringing flux cannot be defined exactly by the analytic method.

V. CONCLUSION

In this study, the parameters of the shunt reactor were succesfully computed by the analytic method. Thanks to the calculated results from the analytic method, a finite element model has been proposed to survey and compare the distributions of the magnetic flux density, inductances (total, leakage, and fringing flux), and energy storage in the gaps, determining the power loss components in the shunt reactor. The error of the calculation results of the total inductance between the two methods is only 0.96%, showing a very good agreement. This test problem can help researchers and manufacturers to standardize the type of iron cores of the shunt reactors in practice.

ACKNOWLEDGEMENT

This work was supported by the Hanoi University of Science and Technology (HUST). The authors also gratefully acknowledge Quy Nhon University for providing the means and conditions needed to carry out this work.

REFERENCES

[1] G. Deb, "Ferranti Effect in Transmission Line," *International Journal of Electrical and Computer Engineering*, vol. 2, no. 4, pp. 447–451, Aug. 2012.

[2] A. Divya Swarna Sri, K. Tejaswini Devi, K. Dhana Raju, and B. Tanya, "Depiction and Compensation of Ferranti Effect in Transmission Line," *International Journal for Research in Applied Science & Engineering Technology*, vol. 6, no. 3, pp. 1522–1526, Mar. 2018, http://doi.org/10.22214/ijraset.2018.3234.

[3] Y. G. Zhang, K. X. Chang, and Y. C. Su, "Shunt Reactors Compensation Research of UHV Accessed to Jiangxi Power Grid," *Advanced Materials Research*, vol. 1070–1072, pp. 1029–1034, 2015, https://doi.org/10.4028/www.scientific.net/AMR.1070-1072.1029.

[4] H, S. Park, B. H. Lee, Y. S. Cho, and S. O. Han, "Calculation of Shunt Reactor Capacity in 400 kV Power System Using EMTP," presented at the International Conference on Electrical Engineering 2006, Korea, Jul. 2006.

[5] K. Dawood, G. Komurgoz, and F. Isik, "Modeling of Distribution Transformer for Analysis of Core Losses of Different Core Materials Using FEM," in *2019 8th International Conference on Modeling Simulation and Applied Optimization (ICMSAO)*, Manama, Bahrain, Apr. 2019, https://doi.org/10.1109/ICMSAO.2019.8880392.

[6] R. Jez, "Influence of the Distributed Air Gap on the Parameters of an Industrial Inductor," *IEEE Transactions on Magnetics*, vol. 53, no. 11, pp. 1–5, Nov. 2017, https://doi.org/10.1109/TMAG.2017.2699120.

[7] S. Pokharel and A. Dimitrovski, "Analytical Modeling of A Ferromagnetic Core Reactor," in *2019 North American Power Symposium (NAPS)*, Wichita, KS, USA, Oct. 2019, https://doi.org/10.1109/NAPS46351.2019.9000352.

[8] E. Kurt, A. Arabul, I. Senol, and F. Keskin Arabul, "An investigation on flux density of three phase distributed Air-Gap 3-5 legged shunt reactor," in *Proceedings of The IRES 21st International Conference*, Amsterdam, Netherlands, Dec. 2015.

[9] I. Uglešić, S. Hutter, M. Krepela, B. Filipović-Grčić, and F. Jakl, "Transients Due to Switching of 400 kV Shunt Reactor," presented at the International Conference on Power System Transients (IPST), Rio de Janeiro, Brazil, 2001.

[10] C.-Y. Lee, C.-J. Chen, C.-R. Chen, and Y.-F. Hsu, "Comparison of transient phenomena when switching shunt reactors on the line's two terminals and station busbar," in *2004 International Conference on Power System Technology, 2004. PowerCon 2004.*, Nov. 2004, vol. 2, pp. 1255–1260, https://doi.org/10.1109/ICPST.2004.1460194.

[11] V. Q. Dang, P. Dular, R. V. Sabariego, L. Krahenbuhl, and C. Geuzaine, "Subproblem Approach for Thin Shell Dual Finite Element Formulations," *IEEE Transactions on Magnetics*, vol. 48, no. 2, pp. 407–410, Feb. 2012, https://doi.org/10.1109/TMAG.2011.2176925.

[12] V. D. Quoc, "Robust Correction Procedure for Accurate Thin Shell Models via a Perturbation Technique," *Engineering, Technology & Applied Science Research*, vol. 10, no. 3, pp. 5832–5836, Jun. 2020, https://doi.org/10.48084/etasr.3615.

[13] V. D. Quoc, "Accurate Magnetic Shell Approximations with Magnetostatic Finite Element Formulations by a Subdomain Approach," *Engineering, Technology & Applied Science Research*, vol. 10, no. 4, pp. 5953–5957, Aug. 2020, https://doi.org/10.48084/etasr.3678.

[14] J. Ning, H. Baoxing, Z. Ruoyu, M. Hongzhong, X. Lei, and L. Li, "Application of Empirical Wavelet Transform in Vibration Signal Analysis of UHV Shunt Reactor," in *2019 IEEE Milan PowerTech*, Milan, Italy, Jun. 2019, https://doi.org/10.1109/PTC.2019.8810623.

[15] Y. Gao, K. Muramatsu, K. Fujiwara, Y. Ishihara, S. Fukuchi, and T. Takahata, "Vibration Analysis of a Reactor Driven by an Inverter Power Supply Considering Electromagnetism and Magnetostriction," *IEEE Transactions on Magnetics*, vol. 45, no. 10, pp. 4789–4792, Oct. 2009, https://doi.org/10.1109/TMAG.2009.2024638.

[16] M. Mu, F. Zheng, Q. Li, and F. C. Lee, "Finite Element Analysis of Inductor Core Loss Under DC Bias Conditions," *IEEE Transactions on Power Electronics*, vol. 28, no. 9, pp. 4414–4421, Sep. 2013, https://doi.org/10.1109/TPEL.2012.2235465.